A new fracture test methodology for the accurate characterization of brittle fracture properties

Aditya Vangal Vasudevan[1], Thiago Melo Grabois[1,2], Guilherme Chagas Cordeiro[2], Romildo Dias Toledo Filho[2] and Laurent Ponson[1] †
[1] *Institut Jean le Rond d'Alembert (UMR 7190), Univeersité Pierre et Marie Curie - CNRS, 4 Place Jussieu, 75005 Paris, France.*
[2] *Laboratorio de Estruturas e Materiais, COPPE/Universidade federal do Rio de Janeiro, CEP 21945-970 RJ, Rio de Janeiro, Brazil.*

Abstract. Crack velocity in rocks is very sensible to the external conditions and has been shown to vary over several orders of magnitude with a slight change in the applied loading. Classical tensile tests such as Compact Tension (CT), Double Torsion (DT) and Double Cantilever Beam (DCB) explore these velocities with a stable crack growth but they are not easily adaptable for rocks. Here we explore a new experimental specimen like a tapered double cantilever beam and we study the kinetics of the crack growth on brittle materials like PMMA. We study systematically the influence of the geometry on the fracture properties using finite elements. We propose a kinetic law relating the fracture energy and the velocity of crack propagation in the form of a power law. Using the kinetic law, we solve numerically the complete crack growth evolution and we are able to predict the Force-displacement($F-\delta$) curve which is in good comparison with the experiments.

Keywords: Crack growth, Stress corrosion, Brittle fracture, Heterogeneous materials, Activation energy

1. Introduction

The Tapered Double Cantilever Beam (TDCB) specimen has been quite popularly used to perform fracture tests for adhesively bonded joints (Marcus and Sih, 1971, Gallagher, 1971, Davalos et al., 1998) and due to the property of having a stable crack growth, it has also been used to study the R-curve behavior in quasi-brittle materials like wood (Coureau et al., 2013). In many experiments it has been observed that for this geometry, the compliance increases linearly with the crack length which have been supported by analytic calculations using beam theory (Davalos et al., 1998, Qiao et al., 2003, Blackman et al., 2003). As the energy release rate (G) depends on the derivative on the compliance (see Eq. 3), when the crack propagates, we have a constant value of G. In our experiments, our focus is not to study the R-curve behavior as our materials are brittle in nature but to have an experimental setup where it would be possible to explore a range of velocities for different fracture energies in one simple test. The classical test geometry used has a straight portion in front of the taper to facilitate the application of the load and the ratio of the width to the length of the specimen is usually less than 0.4. In our specimen we remove this straight portion as having this narrow section for rocks is slightly tedious to machine and the specimen is likely to break in the arms itself. We also explore ratio of width to length of the specimen close to 1 which results in a exponential variation of the compliance with the crack length and hence an exponential decay of fracture energy with crack length,i.e.

† (laurent.ponson@upmc.fr)

increased stability of crack growth and allows us to measure a range of values of fracture energy and velocities for different crack lengths.

2. Materials and methods

2.1. Tapered double cantilever beam

In this study, we focus on a transparent thermoplastic the so called Poly-methyl methacrylate (PMMA) or Plexiglas, an archetype of homogeneous visco-elastic material. Tapered double cantilever beam specimens are obtained machining 8 mm thick PMMA sheets using a laser cutter. In order to help a stable crack propagation and avoid high stress concentration surrounding the initial crack tip position, two ways to sharpen the V shape notch - machined from the cutting process - were designed to initiate fracture: (i) A straight prolongation of approximately 1 millimeter with a razor blade of 0.2 mm thickness and; (ii) a straight prolongation of 3.5 millimeters using the laser cutting process allied to a pre-loading procedure of the sample under a constant 0.5 μm/s crack opening rate up to the exact moment when crack initiates. The sample was then unloaded and the new initial crack length was recorded.

Geometry details are shown in Figure 1(a). As the width of our specimen is relatively thicker (higher width/length ratio), beam theory cannot be effectively applied and we use finite elements (FE) to analyze the sample. We adopt a system where we write the dimensions of the geometry as a multiple of the mesh size of the system. In the FE geometry we use quadrilateral square elements and the mesh size in both - X and Y - directions are denoted as $e_x = e_y$. The geometry of the sample which we have used for our experiments have dimensions $h_1 = 120e_y$ (30 mm), $h_2 = 180e_y$ (45 mm), $L = 400e_x$ (100 mm), $l_x = 51.2e_x$ (12.8 mm) $l_y = 56e_x$ (14 mm) and $R = 10e_y$ (2.5 mm)

For the simulations we use CASTEM an open-source finite element package developed by CEA, France. Exploiting the symmetry in the system, we carry out the simulation just on the upper half of the sample. A typical mesh configuration used in the analysis is shown in Fig. 1. Unit force is applied on the hole for the pins and the displacement is constrained in the Y-direction in the ligament (OA in Fig. 1(a)) to ensure Mode-1 fracture in the specimen. Crack length is increased incrementally and the system is solved for displacements under plane stress and linear elastic conditions. We extract the displacements at the point of application of the force,A (δ_F) and at the location of the clip gauge (δ, B' in Figure 1(a)) and we define a ratio, $r = \delta_F/\delta$. The compliance at these locations are calculated as λ_F and λ and they are related by the same ratio r. We perform all our calculations in our numerical model using the compliance at the point of application of force, but in the experiments, we position the clip gauge at the jaws and hence the displacement and compliance are measured at the jaws of the sample (BB'). We use the ratio , r, to calculate the corresponding displacement at the point of application of the force. We denote by Δ_F and Δ the relative displacements (AA' and BB') and we have assumed a Poisson's ratio of $\nu = 0.3$ in the calculations. However, as we have plane stress conditions, the results of compliance (λ_F)and stress intensity factor(K_I) are independent of the Poisson's ratio.

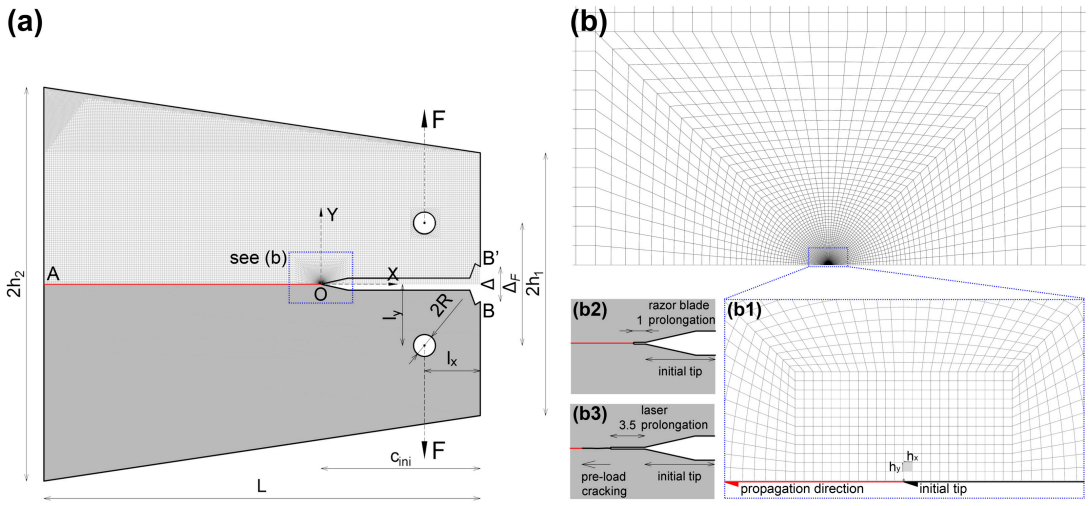

Figure 1. TDCB specimen geometry details: (a) Schematic of the sample with the FE mesh superposed on the upper-half. The mesh is a coarse mesh used for the analyses that has $\sim$ 9x10^3 nodes and $\sim$ 1.8x10^4 dof. The fine mesh used for the analysis has $\sim$ 1.4x10^5 nodes and $\sim$ 2.5x10^5 dof . Figure (b) shows the refinement strategy while (b1) shows the mesh refinement closer to the initial crack tip position of the order of $1e^{-11}$mm. Figures (b2) and (b3) represent the two different strategies for sharpen initial notch: razor blade prolongation and laser prolongation plus pre-load cracking, respectively.

2.2. Finite Element results

A semi-log plot of the non-dimensional compliance and crack length obtained from the finite element solution is shown in Fig. 2. Clearly we see that for a certain range of crack lengths, the dependence of the compliance on the crack length can be fit using an exponential function such as (blue line in Fig. 2):

$$\lambda_F = \frac{\lambda_0}{Eb} e^{c/c_0} \tag{1}$$

where E is the Young's modulus of elasticity, b the thickness of the specimen and λ_0 and c_0 are the parameters of the fit. The compliance follows an exponential fit approximately in the mid-range of crack lengths from $L/3 \lesssim c \lesssim 2L/3$. Once the crack reaches close to the boundary, the ligament is already quite small and the compliance increases very rapidly and it deviates away from an exponential curve (see Fig 2). An alternative route is also suggested to build the compliance vs crack length experimentally by unloading and reloading the experiment as soon as the crack propagates by a few mm. The inverse of the slope in the elastic limit provides the compliance at that respective crack length. The comparison between the normalized compliance results obtained from the experiment and FE result is shown in Figure 2.

We then perform a systematic analysis on the scaling of the parameters of the fit by performing simulations for different geometries. We choose two different geometries (for dimensions see Figure 3) and we vary the length of the specimen. From the inset in Figure 3 we find the parameter c_0 scales only with L and it scales as $c_0 = 0.3886L - 91.5696$ where L is given as a multiple of e_x and λ_0 scales as $\frac{c_0^2}{h_1 l_x}$. We also observe that this scaling is followed only for a limited range being, $60e_x \leqslant l_x \leqslant 90e_x$

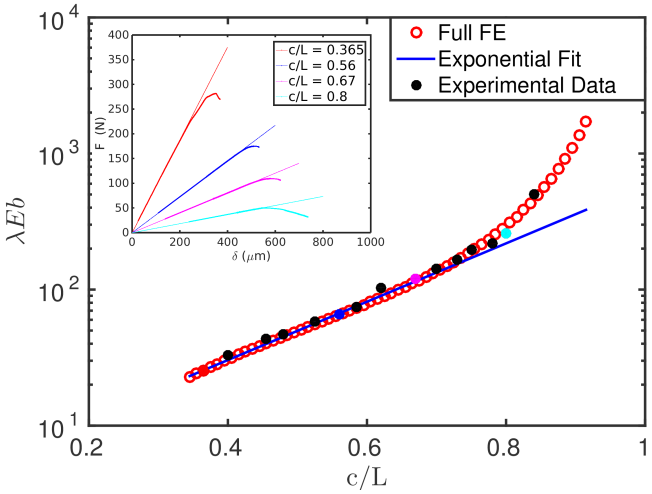

Figure 2. Figure shows the variation of the normalized compliance with crack length. The red circles are the FE results, while the blue line is the exponential fit of the compliance.(Inset) shows the Force-displacement curve for different loaded/unloaded states for the experimental geometry with E = 3 GPa, b = 8mm and the inverse of the slope in the elastic limit gives the compliance which are shown with the respective color in the main plot.

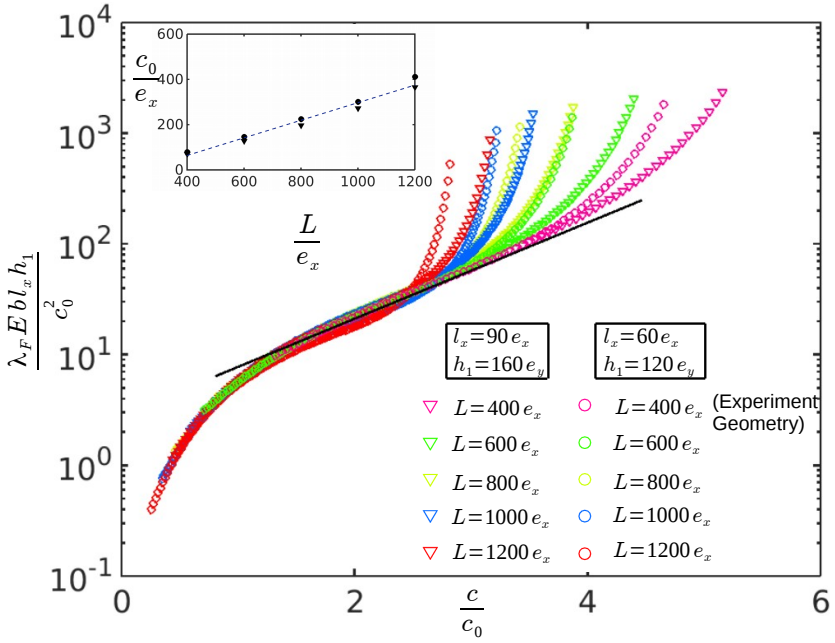

Figure 3. Figure shows the variation of the non-dimensional specimen compliance with non-dimensional crack length for different length of specimens. The simulations are carried out for two different geometries with the same tapering angle α but with different l_x and h_1. Geometry 1 is represented by triangles and has dimensions $l_x = 90e_x, h_1 = 160e_y$ while geometry 2 is represented by circles with dimensions $l_x = 60e_x, h_1 = 120e_y$. The dashed line shows the exponential fit for geometry 2 and length $L = 400e_x$

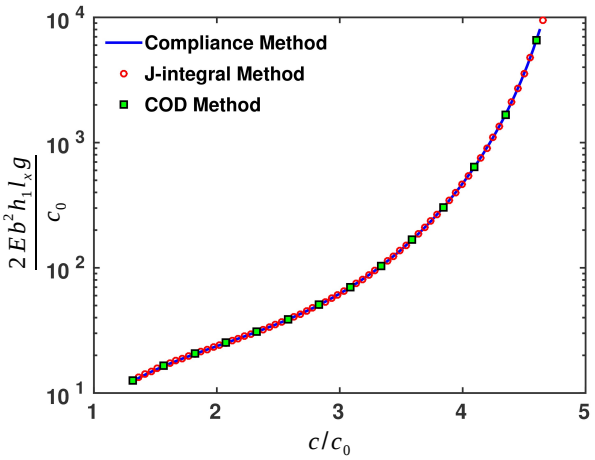

Figure 4. Variation of non-dimensional g as a function of the crack length using different approaches. The figure is plotted for a specimen with $l_x = 22.5$mm, $L = 100$mm and $h_1 = 40$mm

, $120e_x \leqslant h_1 \leqslant 160e_x$ and $400e_x \leqslant L \leqslant 1200e_x$. With this scaling, we see that for different geometries in a given range all the curves for the compliance collapse in the region containing the exponential fit. The compliance for any geometry in this range is then given by

$$\lambda_F \simeq \frac{1}{Eb}\beta\frac{c_0^2}{h_1 l_x}e^{c/c_0} \tag{2}$$

where $\beta \sim 3.0$ from the numerical fit. This is plotted as a dashed line in Figure 3.

From the definition of mechanical energy release rate and simplifying it for a linear elastic material, G is given by the compliance formula, also referred to in literature as the Irwin-Kies equation

$$G = \frac{F^2}{2b}\frac{d\lambda_F}{dc} = F^2 g \tag{3}$$

where g is defined as:

$$g = \frac{1}{2b}\frac{d\lambda_F}{dc} \tag{4}$$

On substituting Eq. 1 in Eq. 4,

$$g = \frac{\lambda_0}{2Eb^2c_0}e^{c/c_0} \tag{5}$$

The inspiration to define a new parameter comes from the fact that g only depends on the geometry of the specimen and G can be decomposed into a product of a term depending on the loading conditions and the geometry. For a unit force and thickness, we have $G = g$. We again plot the non-dimensional value of g on a semi-log scale using the scaling observed with Fig. 3. To verify the value of g we compare it with two other methods viz. the J-integral method and the Crack Opening displacement (COD) method. In the J-integral method, we calculate the energy release rate using the contour integral developed by Rice (Rice, 1968). The contour integral is calculated using

the displacement solution from finite elements and we find the value of G calculated is in accordance with the compliance method. In the COD method we calculate the stress intensity factor by fitting numerically the finite element displacement solution very close to the crack tip. From LEFM, we know that $u(x) \sim K_I\sqrt{x}$, so the stress intensity factor is given by fitting the displacement solution, $u(x)$ with x on a semi-log plot and the intercept of the straight line with slope 0.5 is the stress intensity factor. The energy release rate G is then given by $G = K_I^2/E$ and these values are calculated for different crack lengths and they are in good agreement with the other methods.

As we measure the compliance, we can go from force constant (dead-weight) loading to displacement constant (fixed-grips) loading and back. If we convert equation to fixed grip loading, then we replace F in equation 3 with δ/λ and substituting for λ from Eq. 1, we have

$$G = \frac{\delta_F^2}{\lambda_F^2} g = \delta_F^2 \frac{E e^{\frac{-c}{c_0}}}{2\lambda_0 c_0} \tag{6}$$

From this equation we observe that G decreases exponentially with the increase in crack length, thus allowing us to explore different velocities and fracture energy. Let us now consider other classical fracture tests like Double Cantilever Beam (DCB), Double Torsion and Compact Tension (CT). In DCB and TDCB, the compliance varies as the cube of crack length, and from equation 6 we have the energy release rate varying inversely as the fourth power of crack length (give citation). For the Double Torsion (DT) test, the compliance varies linearly with crack length and the energy release rate varies inversely as the square of crack length (give citation). To have a stable crack growth, it is important that the energy release rate decreases as fast as possible and as the exponential decreases the fastest in comparison to a polynomial function, we will have an extremely stable crack growth.

2.3. Experimental Results

Experiments were carried out in direct uni-axial tension using a Shimadzu (model AG-Xplus) universal testing machine of 10kN maximum load capacity. In this setup, we have a force gauge, i.e. a 1kN load cell, measuring the force at the point of its application (the two holes of diameter 2R in Fig. 2.1(a)) and a clip gauge that measures the displacements between the lips of the crack (Δ in Fig. 2.1(a)). Two steel grips were connected to the specimen by pins placed on its both holes, and the top one pushed up. Experiments were controlled by the the clip gauge opening rate, i.e. by the crack opening displacement (COD) at constant velocity. In this TDCB geometry, the SIF K decreases with the crack length c. A typical $F - \delta$ curve obtained for a PMMA specimen tested at 2.5 $\mu m/s$ COD rate is shown in Figure 5.

2.3.1. *Calculation of crack length and velocity*

To measure the crack length (c(t)) at each time, we use the finite element solution of the specimen, in which we obtain the compliance $\lambda^{\mathrm{FE}}(\mathrm{c})$ at the clip gauge location for different crack lengths. On comparing the compliance obtained from the experiment, $\lambda(\mathrm{t}) = \delta/\mathrm{F}$ with the FE solution ($\lambda^{\mathrm{FE}}(\mathrm{c})$) we can interpolate it to obtain the crack length (c(t)) at each time in the experiment. The crack length normalized w.r.t the length of the sample versus displacement (δ) is plotted in Figure 6. Along with the

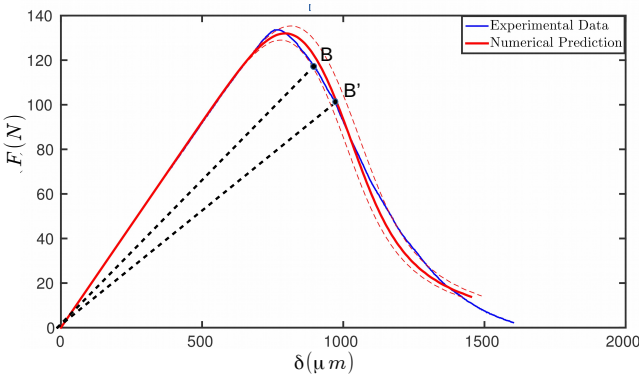

Figure 5. Mechanical behavior of the specimen. Typical load-crack opening displacement curve obtained for the TDCB specimen with the experimental geometry under mode I tensile fracture for PMMA. The blue curve is the experimentally measured curve while the red curve is the theoretically predicted curve with the error bars in red dotted lines.

full FE result, we also plot the crack length predicted by the analytical formula (Eq. 2) and observe a good agreement only till $\frac{c}{L} = 0.7$, which is due to the fact that the compliance as an exponential function of crack length can be written only in a limited range of crack length values ($L/3 \lesssim c \lesssim 2L/3$) The crack growth velocity is then calculated as $v(t) = \frac{dc}{dt}$ which is shown in Figure 7(a). We observe an almost constant crack growth velocity with a slight variation, suggesting the TDCB test is indeed a stable test.

2.3.2. *Calculation of energy release rate (G)*
Once we have the value of crack length, we then have two different methods to calculate the energy release rate, G. In the first method, let us assume at B (in Figure 5) the crack length is c and after time Δt it is $c + \Delta c$ at B'. The mechanical energy release rate is then given by the energy dissipated per unit area of new fracture surface. The energy dissipated during this time interval Δt is equal to the area OBB'O in Figure 5 and the newly created fracture surface area is Δcb where b is the width of the specimen (Morel et al., 2005). Thus, G(t) is then given by

$$G(t) = \frac{E^d(t)}{\Delta c(t) b} \tag{7}$$

where $E^d(t)$ is the energy dissipated (OBB'O). In the second method, we use the full Finite Element solution and use the J-integral method (as elucidated in section2). We compute the energy release rate from both these methods and they are shown in the G-c curve (Fig. 7 (b)). For further analysis, we continue to use the full FE solution from the J-Integral method to calculate the energy release rate (G).

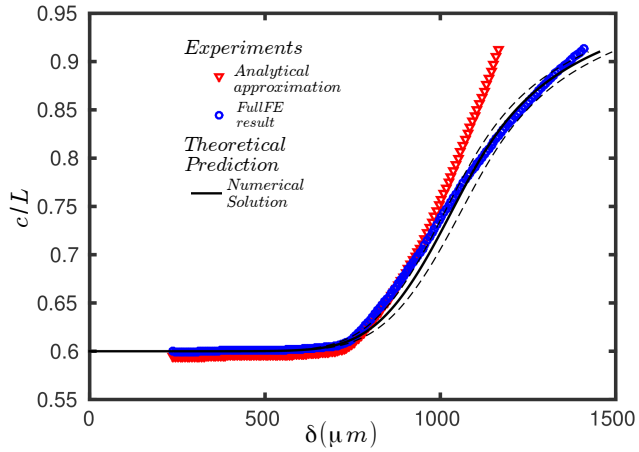

Figure 6. Calculation of crack length by different methods

2.3.3. *Variation of fracture energy, G (J/m^2) with crack velocity* v_m
In polymeric materials like PMMA, for slow crack propagation in polymers the polymeric chains are broken by first gradually elongating the chains which are then broken one-by-one. This elongation process is a rate-dependent process and depends on the velocity at which the crack is propagating in the material and thus the energy released or fracture energy is also dependent on the velocity of crack propagation. The $G_c - v_m$ characteristics is really a material property and for polymeric materials they usually follow a power law. The $G_c - v_m$ dependence for PMMA is shown in Fig. 8 where we clearly see the power law behavior with velocity. From the figure, we also note that with three or four experiments we are able to capture the entire $G_c - v_m$ characteristics, which normally with other classical tests require many more tests. It is also interesting to observe that in one simple test, (for example say test in green dots ($v_e xt = 50\mu m/s$), we explore a range of $G_c - v$ values with the velocity varying atleast 2-3 fold.

2.4. Prediction of average crack velocity (v_m)

From the analytic formula of compliance as an exponential function of crack length, we estimated the average crack growth velocity v_m as a function of the loading rate $\dot{\delta}$. At stable crack propagation, the energy release rate (G) does not vary much with crack length and assuming it as a constant value in Equation 6 we can calculate the crack growth velocity as :

$$v_m = \sqrt{\frac{2Ec_0}{\lambda_0 r G_c}} e^{\frac{-c}{2c_0}} \dot{\delta} \tag{8}$$

where λ_0 and c_0 are parameters obtained from the exponential fit of the compliance (see Equation 1).

Figure 9 shows a log-log plot of the loading rate versus crack growth velocity where we compare the analytical results from equation 8 - for $5e^{-7} \leq \dot{\delta} \leq 1e^{-4}$ $\mu m/s$ - with experimental responses of the average crack growth velocity during stable crack propagation for different loading rate tests. Theoretical and experimental results are

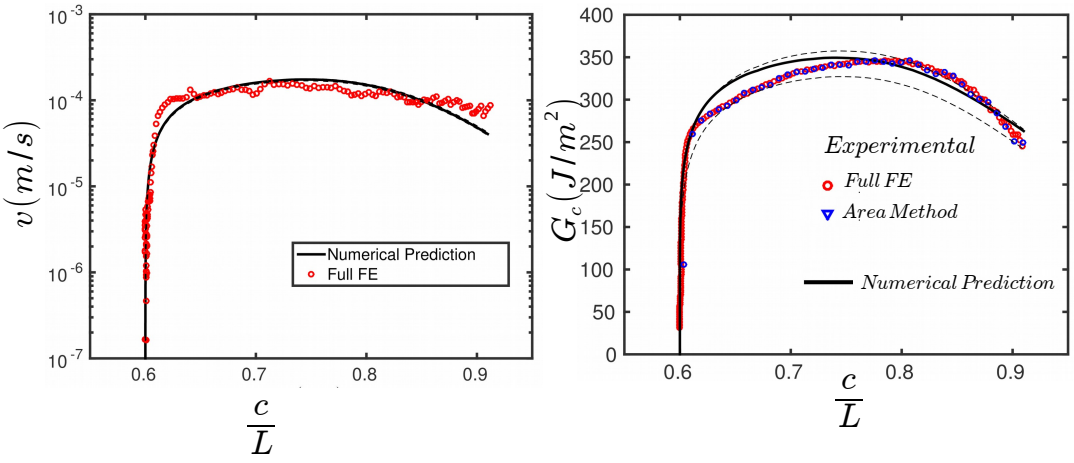

Figure 7. (a) shows the semi-log plot of the variation of crack growth velocity with crack length, comparing results obtained from crack opening displacement measurements plus finite element simulations and numerically predicted solution. (b) shows the $G - c$ plot comparing the Energy release rate calculated from COD+FE and compared with the theoretical curve. The dotted line in both the plots are errorbars from the $G_c - v$ fit.

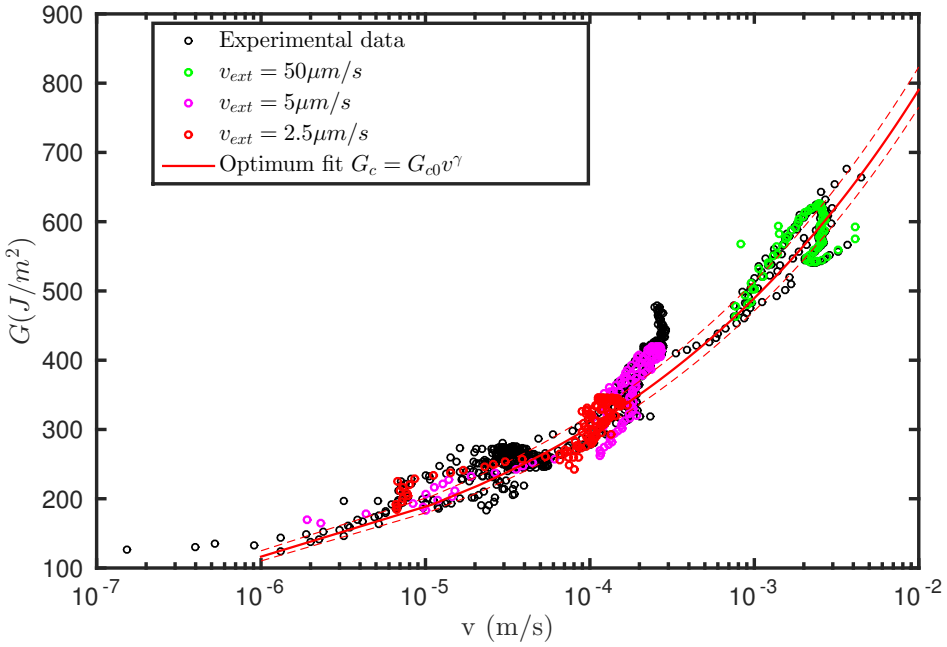

Figure 8. Diagram of energy release rate-crack speed, a ($G-logv_{crack}$) curve at slow crack propagation for brittle fracture.

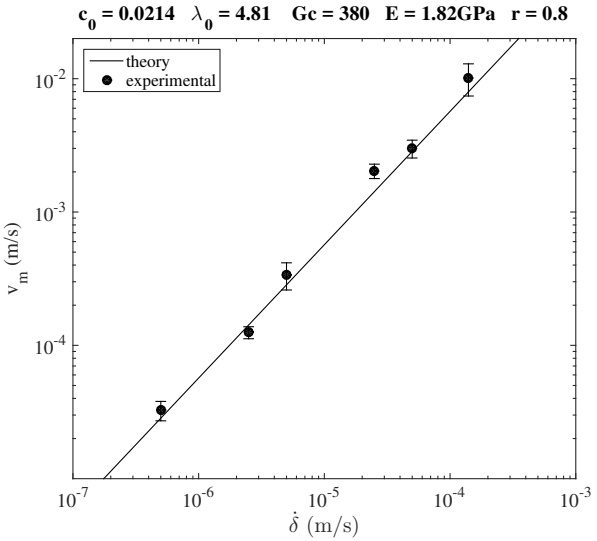

Figure 9. Log-log representation of the average crack velocity-external load correlation function of the experiments. The straight line corresponds to Eq. 8, which the parameters were set to $c_0 = 0.021$, $\lambda_0 = 4.81$, $c = 60mm$, $Gc = 380J.m^{-2}$, $E = 1.82GPa$ and $r = 0.8$.

in agreement proving, therefore, that the analytical formula can be a useful tool to predict crack velocity according the experimental load rate.

3. Determination of the kinetic law $G_c - v$ by optimization

By observing the nature of the $G_c - v$ curve , we assume a power-law behavior of $G_c - v$ as

$$G_c(v) = G_{c0} v^{\gamma} \tag{9}$$

where G_{c0} and γ are parameters of the numerical fit. Thus given a set of parameters G_{c0}andγ for $G_c(v)$, and under static crack propagation we can solve numerically the complete evolution of crack length with time. Using the compliance formula (Eq. 6, we can write static crack propagation law as

$$G = G_c(v_m) \tag{10}$$

$$\Longrightarrow \frac{\delta_F^2}{\lambda_F(c)^2} \frac{d\lambda_F}{dc}(c) = G_{c0} \left(\frac{dc}{dt}\right)^{\gamma} \tag{11}$$

where δ is the displacement imposed at the point of application of the force λ_F is the compliance at the same location. Eq. 11 is a first order equation in time and crack length which is solved numerically to calculate the complete crack growth evolution. Here, for the compliance ($\lambda(c)$), we use the curve obtained from finite elements. Once the crack length is computed, using the compliance vs crack length relation, we can obtain the force as a function of displacement ($F - \delta$) and compare the theoretical $F - \delta$ curve with the experimental curve and they are in good agreement.

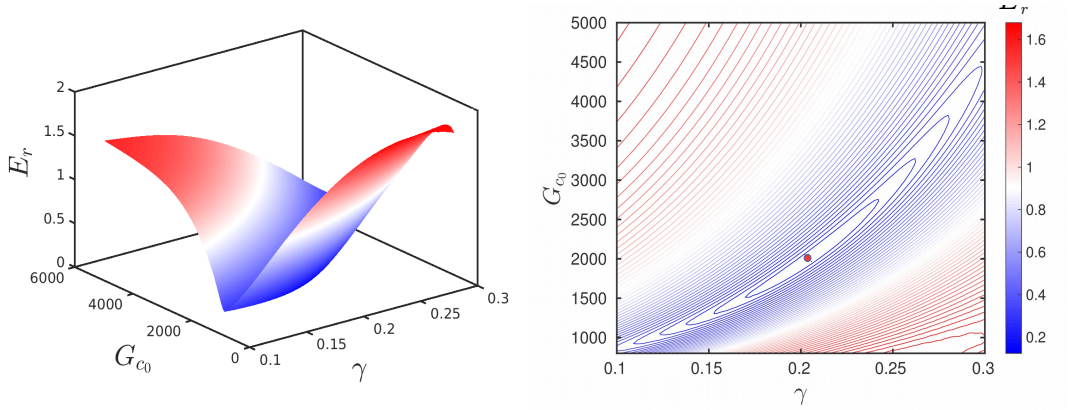

Figure 10. Plot of the error as a function of the optimization parameters

3.1. Calculation of the best parameters G_{c0} and γ of the kinetic law

To have a good correlation between the numerical results and the experimental results, it is important to have the best parameters which fit the $G_c - v$ curve. A slight error in the parameters of the kinetic law can induce a large error in the prediction of the $F - \delta$ curve. We define ϵ_r as the relative error between the numerically predicted force and the experimental value. We define the error in terms of the force as it gives us a direct feedback on the quantities we measure and the quantities we predict. Thus,

$$\epsilon_r = \sqrt{\sum_{\delta_i} \left[\frac{F_{num}(\delta_i) - F_{exp}(\delta_i)}{F_p} \right]^2} \tag{12}$$

where F_p is the half of the peak value of the experimental force and is used to normalize the error.

We choose three different experiments each belonging to a different part of the $G_c(v)$ (shown in different colors in Fig. 8) and define a cumulative error as

$$\epsilon = \sqrt{\frac{\epsilon_1^2 + \epsilon_2^2 + \epsilon_2^2}{3}} \tag{13}$$

We then find a minimum value of the error and find the optimum values of the parameters G_{c0} and γ. The error as a function of γ and G_{c0} is as shown in Figure 10 and we see that there exists a clear minimum, which help in determining the parameters accurately. Once we have an optimum value of the parameters for the kinetic law, using Eq. 11, we can solve for the crack length evolution and a comparison of the numerical prediction and experimentally measured crack length is shown in Figure 6, velocity and fracture energy in Fig. 7 and the dotted lines in each of these graphs are the errorbars by assuming a 10 % error in the parameter optimization.

4. Conclusion

This work reports a combined theoretical and experimental methodology using a new simple geometry to study mode I tensile fracture in brittle materials. We show that the tapering geometry makes the crack growth extremely stable and allows us to measure the energy release rate accurately. Using FE elements, we also show that we have an exponential dependence of compliance with crack length which is why this geometry is really stable. This test is also useful to obtain the $G_c - v$ kinetics of the material as with just a few tests we are able to explore a good range of velocities and energy release rates. We finally also propose an optimization based strategy to calculate the parameters of the $G_c - v$ characteristics using which we are able to predict the fracture properties of the material numerically which are in good accordance with the experiment.

References

Blackman, B., H. Hadavinia, A. Kinloch, M. Paraschi, and J. Williams: 2003, 'The calculation of adhesive fracture energies in mode I: revisiting the tapered double cantilever beam (TDCB) test'. *Engineering Fracture Mechanics* **70**(2), 233 – 248.

Castem, 'CASTEM, a Finite Element package developed by CEA, FRANCE'.

Coureau, J.-L., S. Morel, and N. Dourado: 2013, 'Cohesive zone model and quasibrittle failure of wood: A new light on the adapted specimen geometries for fracture tests'. *Engineering Fracture Mechanics* **109**(0), 328 – 340.

Davalos, J., P. Madabhusi-Raman, P. Qiao, and M. Wolcott: 1998, 'Compliance rate change of tapered double cantilever beam specimen with hybrid interface bonds'. *Theoretical and Applied Fracture Mechanics* **29**(2), 125 – 139.

Gallagher, J.: 1971, 'Experimentally determined stress intensity factors for several contoured double cantilever beam specimens'. *Engineering Fracture Mechanics* **3**(1), 27 – 43.

Marcus, H. and G. C. Sih: 1971, 'A crackline-loaded edge-crack stress corrosion specimen'. *Engineering Fracture Mechanics* **3**(4), 453 – 461.

Morel, S., N. Dourado, G. Valentin, and J. Morais: 2005, 'Wood: A quasi-brittle material. R-curve behavior and peak load evaluation'. *Int. J. Frac.* **131**, 385–400.

Qiao, P., J. Wang, and J. F. Davalos: 2003, 'Tapered beam on elastic foundation model for compliance rate change of {TDCB} specimen'. *Engineering Fracture Mechanics* **70**(2), 339 – 353.

Rice, J.: 1968, 'A path-independant integral and the approximate analysis of strain concentration by notches and cracks'. *J. Appl. Mech.* **35**, 379–386.